Biological and Structural Features of Murine Angiogenin-4, an Angiogenic Protein[†,‡]

Benedict Crabtree, Daniel E. Holloway, Matthew D. Baker, K. Ravi Acharya, and Vasanta Subramanian*

Department of Biology and Biochemistry, University of Bath, Claverton Down, Bath BA2 7AY, United Kingdom

Received October 17, 2006; Revised Manuscript Received November 25, 2006

ABSTRACT: Murine angiogenin-4 (mAng-4) is a member of the pancreatic ribonuclease superfamily that is expressed in some endodermally derived organs. We now show that mAng-4 is angiogenic using a thoracic aorta assay never before applied to the angiogenins. mAng-4, human angiogenin (hAng), and murine angiogenin-1 (mAng-1) stimulate the proliferation of IGR1 melanoma cells but do not stimulate the proliferation or migration of bovine corneal endothelial cells or primary mouse embryonic fibroblasts. In addition, we report the 3-D structure of mAng-4 at 2.02-Å resolution. The structure shows that the residues forming the putative B_1, P_1, and B_2 RNA-binding subsites occupy positions similar to their hAng counterparts. The B_1 subsite is obstructed by Glu115 and Ile118. The obstruction is stabilized by a novel salt bridge between the C-terminal carboxyl group and the side chain of Arg99. Through mutational studies, we identify residues critical to the angiogenic function of mAng-4. The effect of H12A and H112A mutations in the catalytic site indicates that ribonucleolytic activity is essential to angiogenesis. The consequences of a nearby E115A mutation are consistent with a significant role for Glu115 in the attenuation of enzymatic activity but also suggest that sufficient suppression of catalysis is necessary for angiogenesis. The effect of an R32A mutation in the putative nuclear localization sequence indicates that this residue is crucial for angiogenesis. In the putative cell-binding segment, the replacement of Lys59 with Asn (its counterpart at position 61 of hAng) does not abrogate enzymatic activity but abolishes angiogenic activity, the reason for which is unclear.

The angiogenins are monomeric proteins of ∼14 kDa that belong to the pancreatic ribonuclease superfamily (*1*−*3*). Human Ang (hAng[1]), the first Ang family member to be identified (and the one most extensively studied), is an angiogenic factor that induces neovascularization in the chicken chorioallantoic membrane (CAM), rabbit cornea (*4*), and rabbit knee meniscus (*5*). A constituent of normal plasma (*6*) and milk (*7*), it is secreted by a wide variety of normal cells (*3*, *8*) including those of the placenta (*9*, *10*). It has received much attention because of its involvement in the growth of tumors (*11*−*15*). Its expression level is elevated in pancreatic and several other types of cancers (*15*). Antagonists of hAng block tumor growth and metastasis (of prostate cancers in particular) (*11*−*15*), identifying it as a promising target for anticancer therapy.

The interaction of hAng with endothelial cells induces the production of second messengers and the adhesion, migration, and organization of the cells into tube-like structures (*16*−*20*). The mechanism by which hAng induces these changes is partly understood. It first binds to the cell surface, where it interacts with an ∼170 kDa protein (*21*), and it is then internalized and translocated to the nucleolus (*22*). Here, it binds to DNA (*23*) and stimulates the transcription and/or processing of pro-ribosomal RNA (*24*), thereby participating in the increased production of ribosomes essential for cell proliferation. Indeed, the presence of Ang is required for cell proliferation induced by other angiogenic factors, such as basic fibroblast growth factor (bFGF) and vascular endothelial growth factor (*25*). The enzymatic activity of Ang, albeit several orders of magnitude lower than that of RNase A toward conventional RNase substrates (*26*, *27*), is also essential to the angiogenic process (*28*). Mutational and structural studies on hAng have provided much insight into the structural basis of its characteristic enzymatic activity and the aforementioned aspects of its mechanism of angiogenic action (*29*, *30* and references therein, *31*−*33*).

The biological roles of Ang family members may be more far-reaching than was once thought, extending into nervous and immune system function. For example, *Ang* mutations are linked with autosomal dominant familial amyotrophic lateral sclerosis (ALS, a fatal neurodegenerative disorder characterized by the selective destruction of motor neurons)

[†] This work was supported by the Wellcome Trust (UK) through Programme Grant 067288 to K.R.A. and a Postgraduate Studentship to B.C. (073153) under the joint supervision of V.S. and K.R.A.

[‡] The atomic coordinates and structure factors for mAng-4 (codes 2J4T and R2J4TSF, respectively) have been deposited in the Protein Data Bank.

* To whom correspondence should be addressed. Tel: +44-1225-386315. Fax: +44-1225-386779. E-mail: bssvss@bath.ac.uk.

[1] [1]Abbreviations: ALS, amyotrophic lateral sclerosis; Ang, angiogenin; bAng, bovine angiogenin; BAE, bovine aortic endothelial; BCE, bovine corneal endothelial; BSA, bovine serum albumin; bFGF, basic fibroblast growth factor; CAM, chorioallantoic membrane; DMEM, Dulbecco's modified Eagle's medium; ECM, extracellular matrix; FCS, fetal calf serum; GFR, growth factor reduced; hAng, human angiogenin, IT, insulin/transferrin; mAng-1−6, murine angiogenins-1−6; MEF, murine embryonic fibroblast; MTT, 3-(4,5-dimethylthiazol-2-yl)-2,5-diphenyltetrazolium bromide; NEAA, non-essential amino acids; PBS, phosphate-buffered saline; PMNL, polymorphonuclear leukocyte; RNase A, ribonuclease A.

10.1021/bi062158n CCC: $37.00
Published on Web 02/06/2007

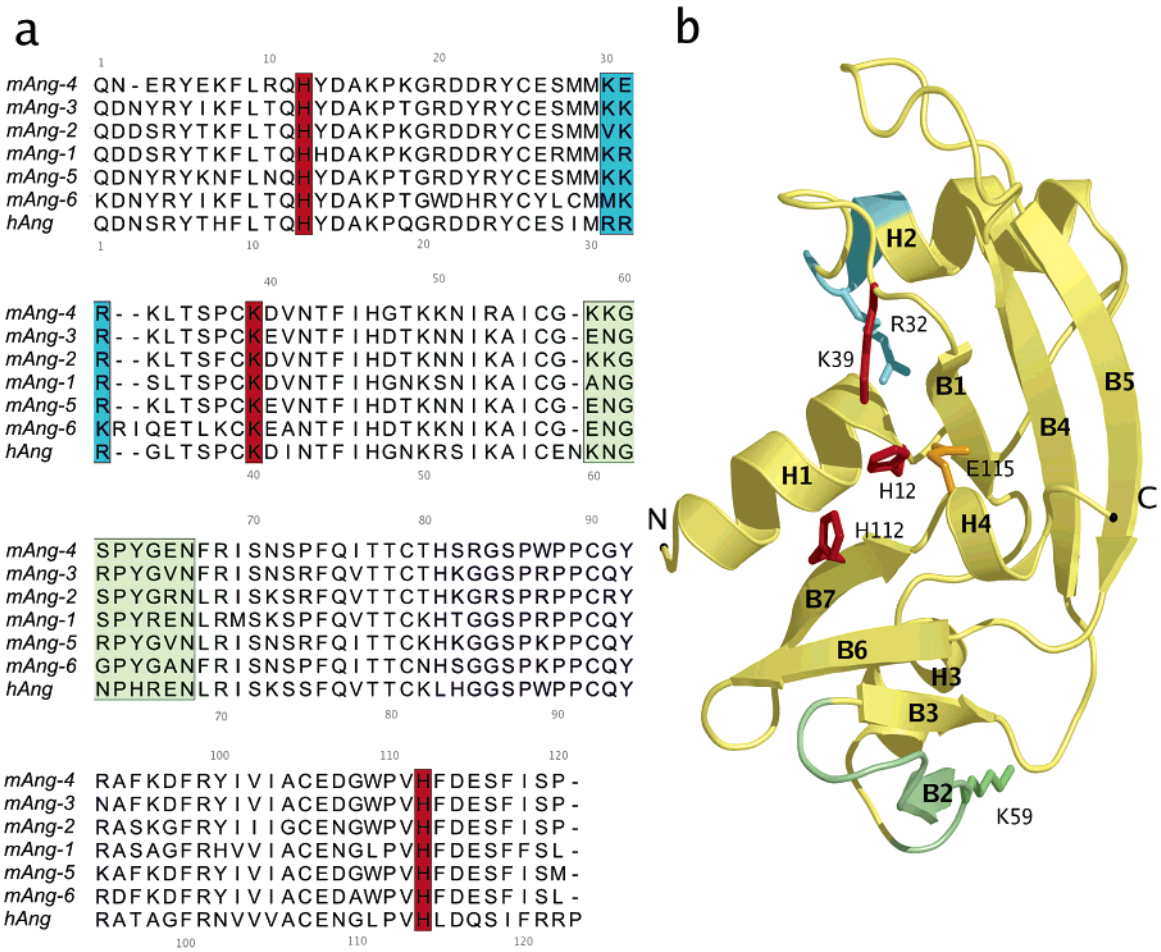

FIGURE 1: Structural overview. (a) Amino acid sequence alignment of human and murine angiogenins. The functional regions of hAng and the aligning regions of the murine proteins are color coded according to the following scheme: red, catalytic triad; cyan, nuclear localization sequence; and green, cell-binding segment. (b) Ribbon diagram of the mAng-4 structure. The residues highlighted in panel a are colored likewise. Side chains of the catalytic triad and other residues mutated in this study are drawn in stick form and labeled. The N- and C-termini and the elements of the secondary structure are also labeled.

and sporadic ALS in individuals of Irish or Scottish descent (*34*, *35*). Synthesis of hAng mRNA is elevated during inflammation, notably in the liver and in the serum during an acute phase response ((*36*), reviewed by Adams and Subramanian (*3*)). hAng has direct anti-microbial activity against systemic bacterial and fungal pathogens (*37*) and yet suppresses the proliferation of mixed lymphocytes (*38*) and inhibits the spontaneous and stimulated degranulation of polymorphonuclear leukocytes (PMNLs) (*39*, *40*).

The physiological and developmental roles of Ang could be studied in greater depth in an experimental organism such as the mouse. hAng's murine orthologue, mAng-1, is highly similar, as judged by amino acid sequence (~76% identity) (*41*) and crystal structure (*42*). However, the murine Ang family has expanded over the course of evolution to include five other members: angiogenin-related protein (mAngRP, renamed mAng-2) (*43*), mAng-3 (*44*), mAng-4 (*45*), mAng-5, and mAng-6 (*46*). The murine angiogenins have 64−93% sequence identity with each other and 55−73% with hAng (Figure 1a). Prior to any gene disruption study, it is desirable to have established the biological activity of each of these proteins and to have identified any functional overlap. At present, it is known that mAng-1 and mAng-3 have angiogenic activities comparable to that of hAng, and that mAng-2 has none (*47*, *48*). mAng-1 is expressed in a wide variety of tissues during and after embryogenesis (Ensembl EST Database, v.40) (*49*), particularly strongly in the placenta and developing nervous system (Subramanian et al., unpublished results). mAng-2 expression has not been reported, whereas mAng-3 expression is evident in the developing embryo (*49*) and in adult prostate and lung tissues (*37*).

The focus of this article is mAng-4. Its angiogenic activity is unknown, and its amino acid sequence has features in common with both angiogenic and non-angiogenic family members, hindering the prediction thereof. Its expression is localized to the gut and pancreas (*49*), and it is up-regulated in the Paneth cells of the gut by the presence of bacteria (*37*). Given that the initial bacterial colonization of the intestine triggers angiogenesis in the mouse and other vertebrates (*50*, *51*), it is possible that mAng-4 is involved in gut angiogenesis. In addition, mAng-4 is selectively toxic to pathogenic gut bacteria, suggesting a role in innate immunity and the regulation of gut micoflora (*37*).

In this article, we present a comprehensive study of the functional and structural properties of mAng-4, a relatively new and uncharacterized member of the angiogenin family. The angiogenic activities of mAng-4 in various biological systems are examined, the X-ray crystal structure is determined, and structure−function relationships are established by site-specific mutagenesis. The findings have important implications for the interpretation of any future murine gene

Table 1: Oligonucleotide Primers Used for the Generation of mAng-4 Mutants

mutation		primers (5′ → 3′)
H12A	sense	CGAAAAATTCCTACGTCAGGCCTATGATGCCAAGCCAAAGG
	antisense	CCTTTGGCTTGGCATCATAGGCCTGACGTAGGAATTTTTCG
R32A	sense	CTGTGAAAGTATGATGAAGGAAGCGAAGCTAACCTCGCCTTGCAA
	antisense	TTGCAAGGCGAGGTTAGCTTCGCTTCCTTCATCATACTTTCACAG
K59N	sense	GGCCATCTGTGGAAAGAATGGAAGCCCTTATGGAG
	antisense	CTCCATAAGGGCTTCCATTCTTTCCACAGATGGCC
H112A	sense	GATGGCTGGCCTGTCGCCTTCGATGAGTCTTTTATCA
	antisense	TGATAAAAGACTCATCGAAGGCGACAGGCCAGCCATC
E115A	sense	GGCCTCCATGCGCGTACCGAGCCTT
	antisense	AAGGCTCGGTACGCGCATGGAGGCC

disruption studies that aim to identify the physiological role of Ang.

EXPERIMENTAL PROCEDURES

Preparation of Angiogenins. [Pyr[1]]-mAng-1, prepared from recombinant *E. coli* W3110 (*47*, *52*), was available from a previous study (*42*), as was an mAng-4 expression plasmid consisting of a copy of the coding sequence inserted into pET-22b(+) (Novagen) (*53*). An hAng expression plasmid comprising a synthetic copy of the coding sequence with *E. coli* codon bias (*54*) inserted into pET-11a (Novagen) was the kind gift of Dr. R. Shapiro (Harvard Medical School, Boston, MA).

Using the oligonucleotides listed in Table 1, the Stratagene QuikChange site-directed mutagenesis kit was used to introduce mutations into a copy of the mAng-4 coding sequence inserted into pBluescriptII KS(+) (Stratagene) (*53*). After confirmation of the mutations by DNA sequencing, expression plasmids were generated by excision of the mutated mAng-4 sequences with *Nde*I and *Bam*HI, and ligation with pET-22b(+).

The hAng expression plasmid was used to transform *E. coli* BL21(DE3) cells, whereas those for mAng-4 and mutants thereof were used to transform *E. coli* BL21-CodonPlus(DE3)-RIL cells (Stratagene). Recombinant proteins in the [Met^{-1}]- form were prepared from these strains by the method of Holloway et al. (*53*). Briefly, expression in shake-flask cultures was induced by the addition of isopropyl-β-D-thiogalactopyranoside, depositing the target proteins in inclusion bodies. These were solubilized, refolded, and purified by SP-Sepharose chromatography followed by C4 reversed-phase HPLC. Purified proteins were lyophilized and dissolved in AnalaR grade water. All mAng-4 mutants behaved in a manner very similar to that of wild-type mAng-4 during purification (*53*), and the purity of each protein was >98% as judged by SDS−PAGE (Figure 2). Protein concentration was estimated using a BCA Protein Assay Kit (Pierce).

Cell Lines and Growth Media. Bovine corneal endothelial (BCE) cells were kindly provided by Dr. G. S. Evans (University of Sheffield, U.K.) and IGR1 melanoma cells by Professor R. Tyrell (University of Bath, U.K.). Primary mouse embryonic fibroblast (MEF) cells were isolated according to standard procedures (*55*) and used at an early passage (P1−P3).

All cell lines were maintained at 37 °C, under 5% CO_2 in a complete medium. For BCE cells, this was Dulbecco's modified Eagle's medium (DMEM)-GlutaMAX supplemented with 10% fetal calf serum (FCS), 1X non-essential amino acids (NEAA), and 5 ng mL^{-1} insulin/10 ng mL^{-1} transferrin (IT) (Invitrogen). For MEF cells, this was DMEM supplemented with 10% FCS and 1X NEAA. For IGR1 cells, this was Earle's minimal essential medium supplemented with 10% FCS, 2 mM L-glutamine, and 25 mM $NaHCO_3$. During assays, a low-serum medium was employed. For all cells, this was the same as the respective complete medium but with the concentration of FCS reduced to 0.1%.

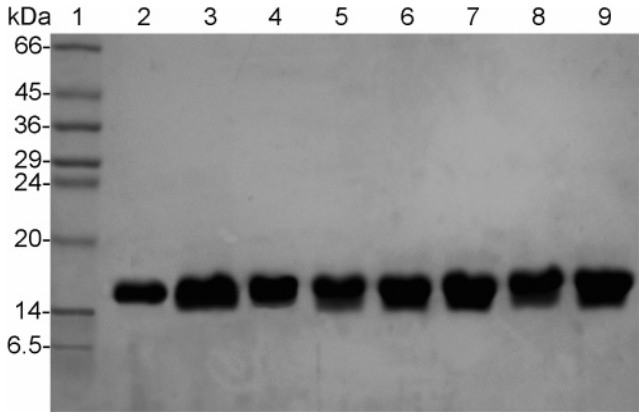

FIGURE 2: SDS−PAGE of purified recombinant human and murine angiogenins. Protein samples were electrophoresed through a 15% polyacrylamide gel and stained with Coomassie Brilliant Blue R-250. Lane 1, molecular mass markers (Sigma); lane 2, hAng; lane 3, mAng-1; lane 4, mAng-4; lane 5, H12A-mAng-4; lane 6, R32A-mAng4; lane 7, K59N-mAng-4; lane 8, H112A-mAng-4; lane 9, E115A-mAng-4.

Angiogenesis Assays. Several different types of angiogenesis assay were employed. In each case, low-serum medium was used as a negative control. Unless stated otherwise, incubations were conducted at 37 °C, under 5% CO_2. All data were analyzed using Student's paired *t*-test.

Cell Proliferation Assay. BCE, MEF, and IGR1 cells in complete medium were used to seed 48-well tissue culture plates (Falcon-BD) at a density of 5×10^3 cells well^{-1}. The cells were incubated for 24 h to allow cell attachment, and the cell layer was washed three times with phosphate-buffered saline (PBS). Low-serum medium supplemented with the test sample (1% FCS, 30 ng mL^{-1} bFGF (R & D Systems), or 200 ng mL^{-1} hAng, mAng-1, mAng-4, or mAng-4 mutant) was then added. Cell proliferation was measured at 24 h intervals over 4 days using a 3-(4,5-dimethylthiazol-2-yl)-2,5-diphenyltetrazolium bromide (MTT) cell proliferation kit (Promega).

Cell Migration Assay. BCE and MEF cells in complete medium were used to seed 6-cm dishes marked with a 2 × 1 cm grid (0.5 cm divisions) at a density of 6×10^5 cells well^{-1}. The cells were grown to confluency (2−3 days) and

the monolayer was scraped in the area of the grid and washed with PBS to remove cell debris. Low-serum medium supplemented with the test sample (30 ng mL^{-1} bFGF or 200 ng mL^{-1} hAng, mAng-1, or mAng-4) was then added. The number of cells migrating into the scraped area was counted at 24 h intervals over 7 days, with the medium being changed every 3 days.

Bead-Based Assay. The organization of BCE cells into tube-like cellular processes was measured using a modification of the bead assay of Nehls and Drenckhahn (*56*). Briefly, BCE cells were grown on Cytodex 3 beads (GE Healthcare) prepared according to the manufacturer's instructions at a density of ~30 cells bead^{-1}. Incubation continued for 48 h until the cells were confluent. The cell-coated beads were washed in low-serum medium, incubated for a further 1 h, then embedded in growth factor-reduced (GFR) Matrigel (BD Biosciences) that had been freeze-thawed twice prior to use. Low-serum medium containing 40 beads was mixed with an equal volume of GFR Matrigel (50% (v/v) in ice-cold low-serum medium), added to a well of an 8-well chamber slide and incubated for 30 min to allow the GFR Matrigel to set. Low-serum medium supplemented with the test sample (30 ng mL^{-1} bFGF or 100 ng mL^{-1} hAng, mAng-1, or mAng-4) was then added. Incubation was continued for 5 days, during which time daily observations were made using a Nikon inverted microscope. On day 5, the beads were fixed with paraformaldehyde (4% in PBS, 15 min) and stained with bis-benzimide (Hoechst 33258) (20 μg mL^{-1} in PBS, 1 h), all at room temperature. The number of outgrowths from each bead was counted. An outgrowth was considered a process when it was longer than 150 μm (the diameter of a Cytodex 3 bead) and consisted of three or more cells (*56*).

Thoracic Aorta Assay. The response of pre-existing vasculature was measured using a thoracic aorta assay (*57*). Aortae were isolated from 6−8-week-old MF1 female mice, cleaned, and flushed with MCDB131 medium (Invitrogen) containing 100 U mL^{-1} penicillin and 100 μg mL^{-1} streptomycin (Sigma). Prior to use, GFR Matrigel was diluted 1:1 with a low-serum MCDB131 medium consisting of MCDB131 supplemented with 0.1% murine serum (Autogen Bioclear), 100 U mL^{-1} penicillin, 100 μg mL^{-1} streptomycin, 2 mM L-glutamine, and 25 mM $NaHCO_3$, and kept on ice. Cross-sectional slices of aorta were sandwiched between 50 μL layers of polymerized GFR Matrigel in the wells of 8-well chamber slides. These were incubated for 30 min to allow the GFR Matrigel to set, after which time the low-serum MCDB131 medium supplemented with test protein (50, 100, or 200 ng mL^{-1} hAng, mAng-1, mAng-4, or mAng-4 mutant) was added to each well. Incubation was continued for 5 days, during which time daily observations were made, and the number of cellular processes per aortic section was recorded. For each sample, a section from the same aorta was tested to minimize the biological variation between mice.

Ribonucleolytic Activity Assay. tRNA cleavage assays were conducted as described by Shapiro et al. (*58*) except that the buffer was 33 mM Na-Hepes at pH 7.0 and incubations were for 2 h. Assays contained 2 mg mL^{-1} yeast tRNA (Sigma), 0.1 mg mL^{-1} bovine serum albumin (BSA), and, unless stated otherwise, 0−0.5 μM test protein. The reaction was terminated by the addition of 2 vol ice-cold 3.4% perchloric acid and centrifuged at 13000*g* for 10 min at 4 °C. The A_{260} of the supernatant was used as a measure of RNase activity. The magnitude of the activity in the quasi-linear portion of each plot (0.2−0.3 μM protein) was used in the calculation of relative activities. By this means, the activities of mAng-1 and mAng-4 were 26 and 18% of that of hAng, respectively (Figure 3a), in accordance with previous measurements (*47*, *53*). For the superactive E115A-mAng-4 mutant, the protein concentration range assayed was reduced 20-fold. The activity in the quasi-linear portion of the plot (0.010−0.015 μM protein) was then multiplied 20-fold to provide a comparison with the activity of wild-type mAng-4.

Table 2: Crystallographic Statistics

diffraction data	
space group	*C*2
unit cell parameters	$a = 97.5$, $b = 31.4$, $c = 95.5$ Å, $\beta = 118.9°$
resolution range (Å)	50−2.02
no. of reflections	
measured	57865
unique	17076
R_{symm}[a]	0.14 (0.52)[b]
$I/\sigma(I)$	11.3 (2.8)[b]
completeness (%)	74.2 (49.1)[b]
refined model	
R_{cryst}[c]	0.232
R_{free}[d]	0.294
deviation from ideality (rms)	
bond lengths (Å)	0.006
bond angles (deg)	1.42
no. of atoms	
protein	962, 965[e]
water	76
mean *B*-factor (Å^2)	
protein	38.2, 38.5[e]
water	39.7

[a] $R_{symm} = \Sigma_h\Sigma_i[|I_i(h) - \langle I(h)\rangle|/\Sigma_h\Sigma_i I_i(h)]$, where I_i is the i^{th} measurement and $\langle I(h)\rangle$ is the weighted mean of all measurements of $I(h)$. [b] Figures in parentheses refer to the outermost shell (2.09−2.02 Å). [c] $R_{cryst} = \Sigma_h|F_o - F_c|/\Sigma_h F_o$, where F_o and F_c are the observed and calculated structure factor amplitudes of reflection *h*, respectively. [d] R_{free} is equal to R_{cryst} for a randomly selected 5% subset of reflections not used in the refinement (*62*). [e] Molecule A, molecule B.

X-ray Crystallography. mAng-4 crystals were grown at 16 °C by the hanging drop-vapor diffusion method. Initial, twinned crystals were grown by mixing equal volumes of protein solution (8 mg mL^{-1} in water) and reservoir (25% PEG 3350, 0.2 M Li_2SO_4, and 0.1 M Tris-HCl at pH 8.5). These crystals were used to seed preequilibrated drops containing 4 mg mL^{-1} protein, 20% PEG 3350, 0.05 M Li_2SO_4, and 0.09 M Tris-HCl at pH 8.5. Crystals were transferred briefly to a cryoprotectant composed of reservoir solution supplemented with 25% glycerol before the collection of diffraction data at 100 K. Data were collected using an ADSC Quantum-4 CCD detector on station PX 14.1 at the Synchrotron Radiation Source (Daresbury, U.K.). All data were processed and scaled using the HKL suite (*59*). The asymmetric unit contained two mAng-4 molecules (designated A and B). Detailed processing statistics are given in Table 2.

For structure determination, molecular replacement was performed with AMoRe (*60*), employing a search model derived from the coordinates of hAng (pdb entry 1B1I) (*30*). In this search model, all non-glycine residues that differed from their counterparts in mAng-4 were replaced with alanine. Refinement was carried out using CNS (*61*) with

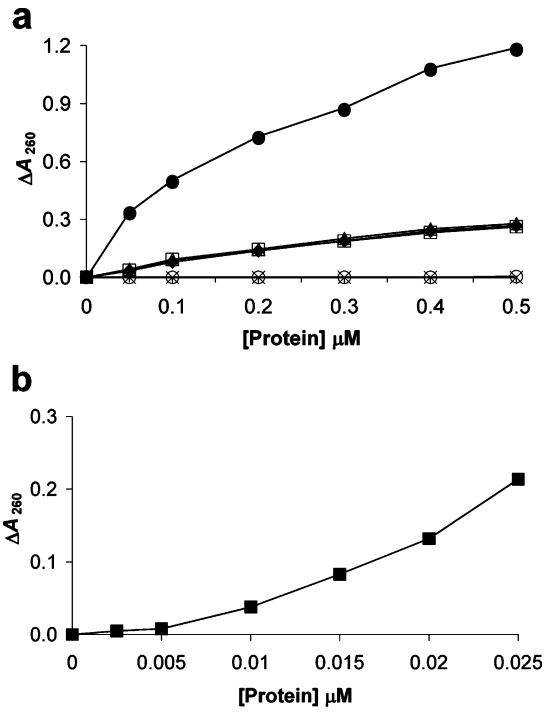

FIGURE 3: Ribonucleolytic activities of hAng, mAng-4, and mAng-4 mutants. (a) Activities of hAng (●), mAng-4 (◆), H12A- (×), R32A- (Δ), K59N- (□), and H112A-mAng-4 (○). (b) Activity of E115A-mAng-4 (■). Assays were conducted for 2 h at 37 °C in 33 mM Na-HEPES at pH 7.0 and 33 mM NaCl, and contained 2 mg mL^{-1} yeast tRNA, 0.1 mg mL^{-1} BSA, plus the indicated concentrations of recombinant protein. At the end of the incubation period, the absorbance of perchloric acid-soluble fragments was determined as described (*58*). Each data point represents the mean of six measurements. In all cases, the standard deviation is less than 2% of the mean and is inconveniently small to display as an error bar.

5% of the reflections set aside for cross-validation (*62*). After an initial round of rigid-body refinement, cycles of energy minimization, individual *B*-factor refinement, simulated annealing, and electron density map calculation were interspersed with manual model building using O (*63*). Water molecules were added using the water_pick protocol assuming a minimum $F_o - F_c$ peak height of 3σ. Final models were analyzed and validated using the WHAT_CHECK (*64*), PROCHECK (*65*), BAVERAGE, and SUPERPOSE modules of the CCP4 suite (*66*) and MOLPROBITY (*67*). Detailed statistics for the model are presented in Table 2. Figures were drawn using PyMOL (DeLano Scientific, San Carlos, CA) and CCP4mg (*68*).

RESULTS

Angiogenic Activity of mAng-4. The angiogenic activity of mAng-4 was assessed using a range of assays designed to measure its ability to stimulate different aspects of angiogenesis, namely, cell proliferation, migration, and the formation of cellular processes.

The proliferative response was measured using two nontransformed cell lines (BCE and MEF) and one malignant cell line (IGR1 human melanoma). BCE cells proliferated in response to 1% FCS ($p < 0.05$; $n = 5$), whereas MEF cells responded to 30 ng mL^{-1} bFGF ($p < 0.01$; $n = 5$) (Figure 4a and b). However, neither of these cell lines proliferated in response to 200 ng mL^{-1} hAng, mAng-1, or mAng-4 (Figure 4a and b). In contrast, IGR1 cells, which

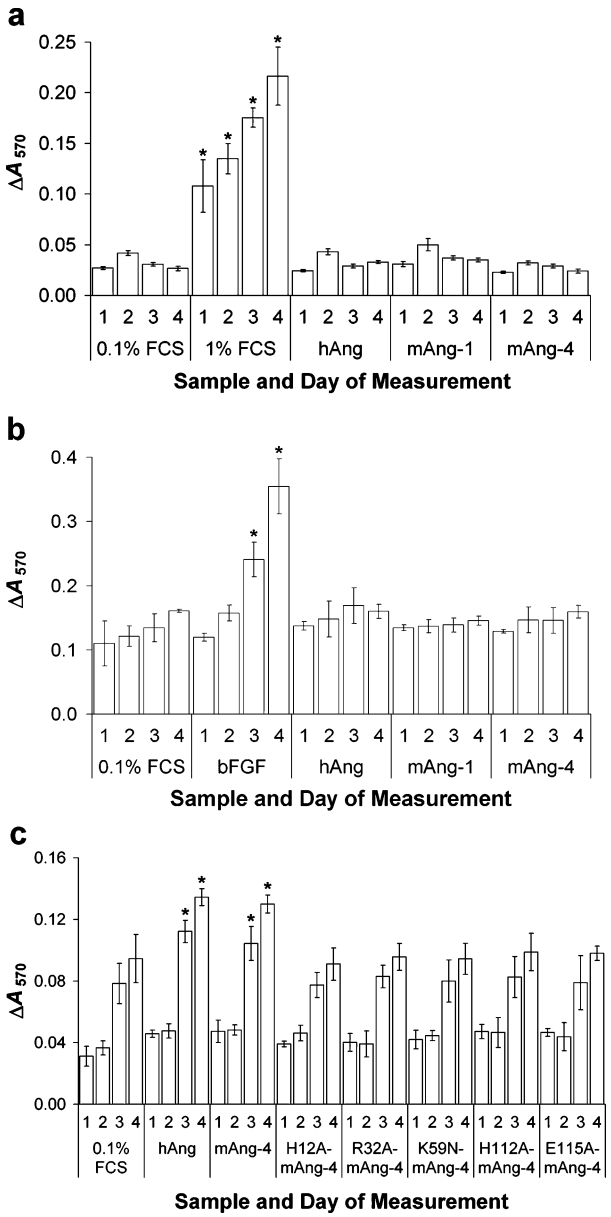

FIGURE 4: Proliferative activities of hAng, mAng-1, mAng-4, and mAng-4 mutants. Histograms showing the mean proliferation (±SD) of (a) BCE, (b) MEF, and (c) IGR1 cells in response to the indicated substances as determined by MTT assay. In each case, the negative control was 0.1% FCS. Angiogenins were assayed at 200 ng mL^{-1} and bFGF (positive control for MEF cells) at 30 ng mL^{-1}, all in the presence of 0.1% FCS. Asterisks denote values that differ from those of the corresponding negative control samples by a statistically significant margin.

were able to proliferate to a degree in low-serum medium, showed a significantly greater proliferation in response to either 200 ng mL^{-1} hAng or mAng-4 ($p < 0.004$ and 0.007, respectively; $n = 5$) (Figure 4c).

The ability to trigger cellular invasion of an area cleared of cells by scraping, that is, a wounding response, was tested over a 7 day period with BCE and MEF cells. bFGF stimulated a migration into the wounded area that was significantly stronger than that in the negative control ($p < 0.01$ and 0.001 for BCE and MEF cells, respectively; $n = 21$) (Figure 5). However, hAng, mAng-1, or mAng-4 did not stimulate any such migration (Figure 5).

The induction of cellular processes from BCE cell-coated Cytodex 3 beads embedded in GFR Matrigel was assessed.

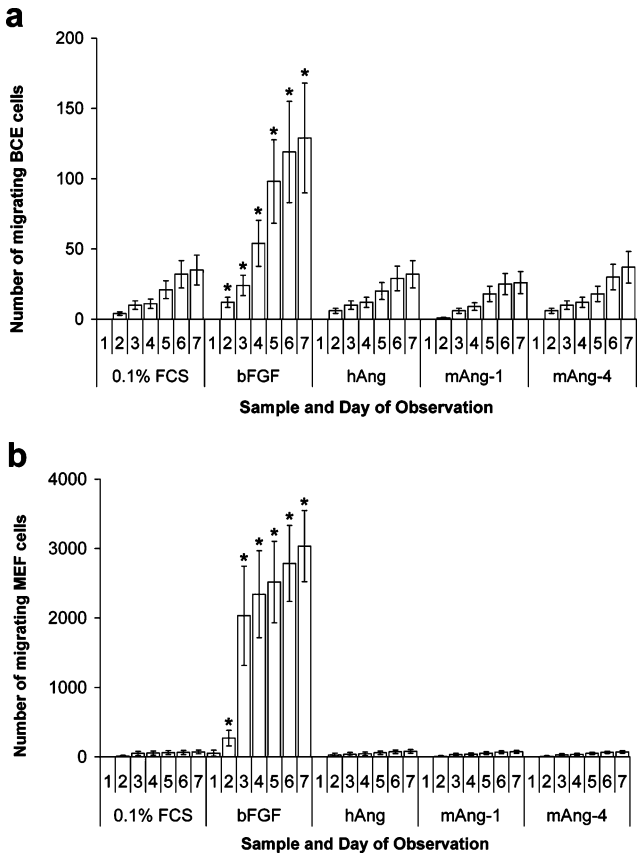

FIGURE 5: Wound healing activities of hAng, mAng-1, and mAng-4. Histograms showing the mean number (±SD) of (a) BCE and (b) MEF cells migrating in the presence of the indicated substances on days 1−7 after scraping a 2 × 1 cm^2 area clear of cells. In each case, the negative control was 0.1% FCS. Angiogenins were assayed at 200 ng mL^{-1} and bFGF (positive control) at 30 ng mL^{-1}, all in the presence of 0.1% FCS. Asterisks denote values that differ from those of the corresponding negative control samples by a statistically significant margin.

The cells adhered well to Cytodex 3 beads (Figure 6). Freeze-thawing the GFR Matrigel twice effectively suppressed sprouting in the negative control (Figure 6a). The cells formed an extensive network of processes in response to 30 ng mL^{-1} bFGF (7.0 ± 0.2 processes bead^{-1}; $n = 100$), indicating that the cells were healthy and that GFR Matrigel could support the required morphogenesis (Figure 6b). However, hAng, mAng-1, or mAng-4 did not induce the formation of any such outgrowths (Figure 6c−e).

The induction of cellular processes was also measured using thoracic aortae embedded in GFR Matrigel. The negative control showed negligible process formation, whereas hAng and mAng-1 strongly induced process formation at 50, 100, and 200 ng mL^{-1} (at the highest concentration, $p < 0.00002$ and 0.0002, respectively; $n = 10$) (Figure 7a−d). Well-defined cellular processes appeared on day 2 or 3 of incubation and increased rapidly on subsequent days. They grew from the periphery of the section, extended out into GFR Matrigel, and had a branching morphology, indicating their endothelial nature. Over the 5 day assay period, a dense network formed. As the concentration of hAng or mAng-1 was increased, it appeared that the cellular response also increased, but the effect was not statistically significant.

mAng-4 stimulated the formation of cellular processes from thoracic aortae at 50, 100, and 200 ng mL^{-1} (at the highest concentration, $p < 0.0001$; $n = 10$) (Figure 7a and e). The time course of the response was the same as that observed with hAng and mAng-1 (processes appeared on day 3), as was the manner in which the response reflected the concentration applied. Among the angiogenins tested, hAng appeared to have the most potent activity. At 200 ng mL^{-1}, the relative activities of mAng-1 and mAng-4 were 82 and 61% of that of hAng, respectively, but the differences are not statistically significant.

Overview of the mAng-4 Structure. The crystal structure of mAng-4 was determined at 2.02 Å resolution. The crystals contained two molecules in the asymmetric unit (A and B), and the final model comprises residues 2−120 of each. The C$^\alpha$ atoms of molecules A and B do not differ significantly (rms deviation = 0.54 Å), nor do the side chain positions. Hence, molecule A will be referred to throughout the text unless stated otherwise.

mAng-4 adopts the familiar α/β-fold of RNase A and other members of the Ang family (Figure 1b). The main chain is well ordered in both molecules apart from at residues 84−89 in the region of the B4−B5 loop. High flexibility of the corresponding loop is a characteristic of RNase A family members, and it is also poorly defined in the crystal structures of hAng and mAng-1 (*30*, *42*). The Ramachandran plot reveals that 83.2% of residues lie in the most favored regions with the remainder in the other allowed regions. The main chain conformation is very similar to that of hAng (pdb entry 1B1I) (*30*) and mAng-1 (pdb entry 2BWK) (*42*). When C$^\alpha$ atoms are aligned, residues 4−118 deviate from their mAng counterparts (residues 5−119) by 0.78 Å, and residues 3−120 deviate from their hAng counterparts (residues 4−58 and 60−122)[2] by 0.81 Å (rmsd). The greatest differences are found in relatively unconstrained regions of the model, namely, the termini and the H1−H2, H2−B1, H3−B2, B2−B3, and B4−B5 loops.

Substrate-Binding Subsites. Pancreatic ribonuclease superfamily members employ a catalytic triad of residues to specifically cleave RNA on the 3′-side of pyrimidine nucleotides (*69*). Pyrimidine bases bind to an enzyme subsite designated B_1, whereas the adjacent scissile phosphodiester linkage binds to P_1 (which includes the catalytic triad), and the base immediately downstream (preferentially a purine) binds to B_2 (*70*). The residues that are believed to form the B_1, P_1, and B_2 subsites of hAng and mAng-1 (*30* and references therein, *42*) are conserved strongly in the sequence of mAng-4. In the mAng-4 structure, His12, Lys39, and His112 adopt positions consistent with their identity with the catalytic triad and, along with the side chain of Gln11 and the main chain O atom of Phe113, are positioned to form the P_1 subsite.

Residues that are likely to form the B_1 subsite (His12, Val41, Asn42, Thr43, and Phe113) are conventionally positioned. As observed in the structures of other Ang family members (*29*, *42*, *71*), the B_1 subsite is obstructed by the C-terminal segment (residues 115−120 of mAng-4), and a major rearrangement of the C-terminal segment is the only

[2] Compared to hAng, all murine angiogenins have a 1-residue deletion in the H3−B2 loop. In mAng-4, this falls at position 59, hence the omission of this residue from the alignment.

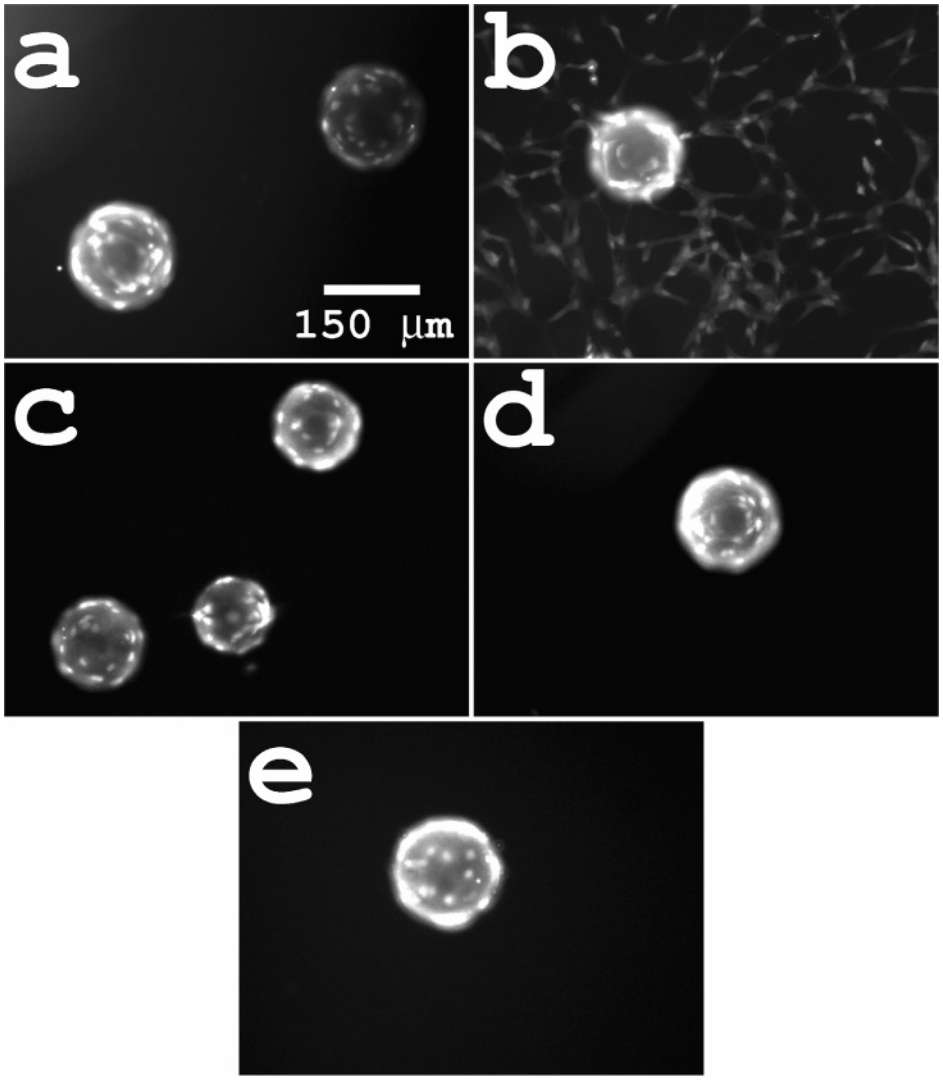

FIGURE 6: Morphology of BCE cell-coated Cytodex 3 beads after exposure to hAng, mAng-1, and mAng-4. GFR Matrigel-embedded BCE cell-coated Cytodex 3 beads, stained with Hoechst 33258 and photographed after a 5-day exposure to 0.1% FCS plus (a) nothing (negative control), (b) 30 ng mL^{-1} bFGF (positive control), (c) 100 ng mL^{-1} hAng, (d) 100 ng mL^{-1} mAng-1, and (e) 100 ng mL^{-1} mAng-4. The bar represents 150 μm.

reasonable means by which RNA substrates can bind productively (Figure 8a). Glu115 mimics part of a pyrimidine ring, spanning the B_1 subsite in the manner of its hAng and mAng-1 counterparts (Gln117 and Glu116, respectively) to engage in hydrogen bonds with main and side chain atoms of Thr43. The side chain of Ile118 is also obstructive, contributing to an extensive set of hydrophobic interactions between the C-terminal segment and the main body of the protein. Because of the presence of Phe residues at positions 113 and 117 (a feature found in the corresponding part of mAng-1 but not hAng), the C-terminus−main body packing arrangement more closely resembles that of mAng-1 than that of hAng. As postulated for mAng-1 (*42*), this relatively tight arrangement may contribute to the relatively low ribonucleolytic activity of mAng-4 among angiogenins. The obstructive position of the C-terminal segment is also stabilized by a salt bridge between the carboxyl group of the C-terminal residue, Pro120, and the guanidino group of Arg99 (Figure 8a). This feature is not present in hAng, mAng-1, or bAng and may serve to further suppress ribonucleolytic activity.

The B_2 subsite of angiogenins in general has not been well defined and may be rather rudimentary. Residues that could conceivably form the B_2 subsite of mAng-4 (Phe67, Ala104, and His112) occupy positions similar to those of their counterparts in hAng and mAng-1.

Nuclear Localization Sequence. Three consecutive positively charged residues (Arg31−Arg32−Arg33) comprise a crucial element (and most probably the whole) of the nuclear localization sequence (NLS) of hAng (*72*) (Figures 1a and 8b). Arg33 is essential for nuclear targeting, whereas Arg31 and Arg32 play a modulatory role. The corresponding segment of mAng-4 has a different sequence: Lys30−Glu31−Arg32. The backbone conformation and side chain positions of mAng-4 and hAng are well conserved in this region, but the surface charge distribution differs because of the substitution of Glu31 for Arg32 (Figure 8c). Although a consecutive run of positive charges is absent from the mAng-4 structure, novel substitutions (Arg10 for Thr11, Lys33 for Gly34, and Lys7 for His8) provide extra positive charges in the immediate vicinity and form a novel basic patch. This patch may comprise a noncontiguous monopartite

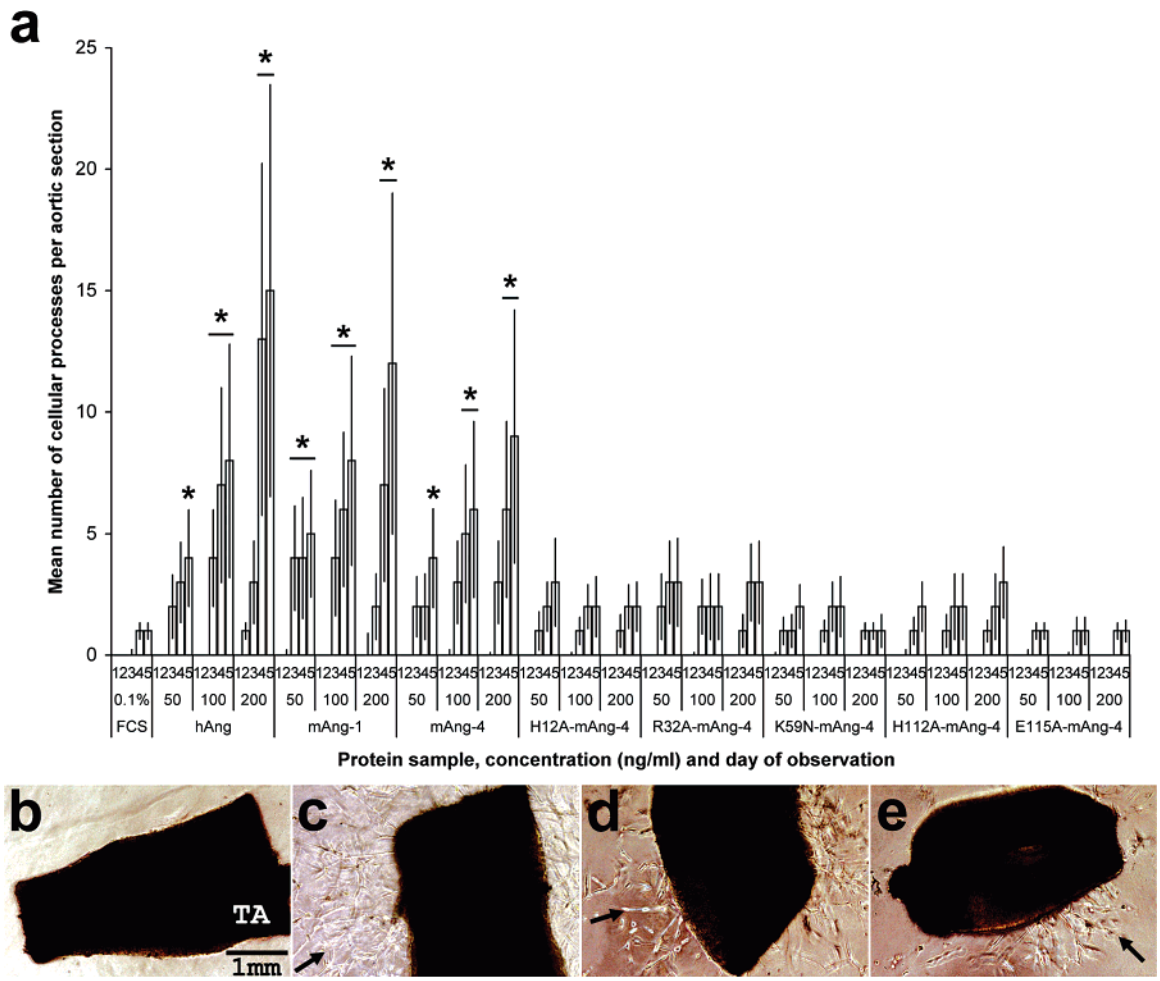

FIGURE 7: Angiogenic activities of hAng, mAng-1, mAng-4, and mAng-4 mutants as determined by the thoracic aorta assay. (a) Histograms showing the mean number (±SD) of cellular processes growing from thoracic aorta sections on days 1−5 in the presence of 0.1% FCS plus nothing (negative control) or 50, 100, and 200 ng mL^{-1} of the indicated angiogenins. Asterisks denote values that differ from those of the corresponding negative control samples by a statistically significant margin. Also shown are thoracic aorta (TA) sections, photographed after a 5-day exposure to 0.1% FCS plus (b) nothing (negative control), (c) hAng, (d) mAng-1, and (e) mAng-4, all at 200 ng mL^{-1}. The arrows indicate regions where cellular processes have formed. The bar represents 1 mm.

NLS, or taking into account the abundance of basic residues on the surface of mAng-4, it may contribute to a bipartite NLS (*73*). Although it would be unusual, it is also possible that the whole Lys30−Glu31−Arg32 segment contributes to the NLS because there is scope for the inclusion of acidic residues (*73*).

Cell-Binding Site. Residues 60−68 and Asn109 of hAng have been implicated in cell binding (*52*, *74*, *75*). The 60−68 segment comprises a short β-strand (B2) and parts of the two flanking loops, and is well conserved in mAng-1 but less so in other murine angiogenins including mAng-4 (Figure 1a). Structural modification of hAng Asn61 (to isoAsp or Asp) or Arg66 (to Ala) has no appreciable effect on enzymatic activity but abolishes angiogenic activity. The resulting proteins do not inhibit wild-type hAng-induced neovascularization, signifying the importance of these two residues to cell binding and a low tolerance of their modification (*52*, *75*). In mAng-1, these residues are preserved, but in mAng-4, they are replaced with Lys59 and Gly64, respectively. When the structure of mAng-4 is compared with those of hAng and mAng-1, the effects of these changes are revealed (Figure 8d). The C^{α} trace of the mAng-4 segment (residues 58−66) more closely resembles that of mAng-1 (residues 59−67) than that of hAng, the rms deviations being 0.47 and 1.0 Å, respectively. This is chiefly because all murine angiogenins have a single Gly residue in place of the Glu−Asn sequence found in hAng immediately upstream of the segment, altering the position of the first residue. Indeed, the C^{α} atom of Lys58 deviates from that of its hAng counterpart (Lys60) by 1.9 Å, although both side chains are oriented toward the solvent. At position 59, the Asn → Lys substitution introduces an extra positive charge to the region. Lys59 extends out into the solvent, matching its mAng-1 counterpart (Asn60) but differing from its hAng counterpart (Asn61), which instead faces inward and engages in intramolecular hydrogen bonds. The positions and conformations of residues 60−63 are very similar to those of their hAng and mAng-1 counterparts because of their conserved β-structure. The Arg → Gly substitution at position 64 removes a positive charge and increases the torsional freedom at this point, allowing residues Gly64, Glu65, and Asn66 to deviate slightly from the equivalent residues of hAng and mAng-1. The orientations of the Glu65 and Asn66 side chains broadly match those of their counterparts (i.e., toward the solvent), but there is no new positive charge in the immediate vicinity to compensate for the Arg → Gly substitution. The structure of mAng-4 confirms that the substitution of the key hAng residues Asn61 and Arg66

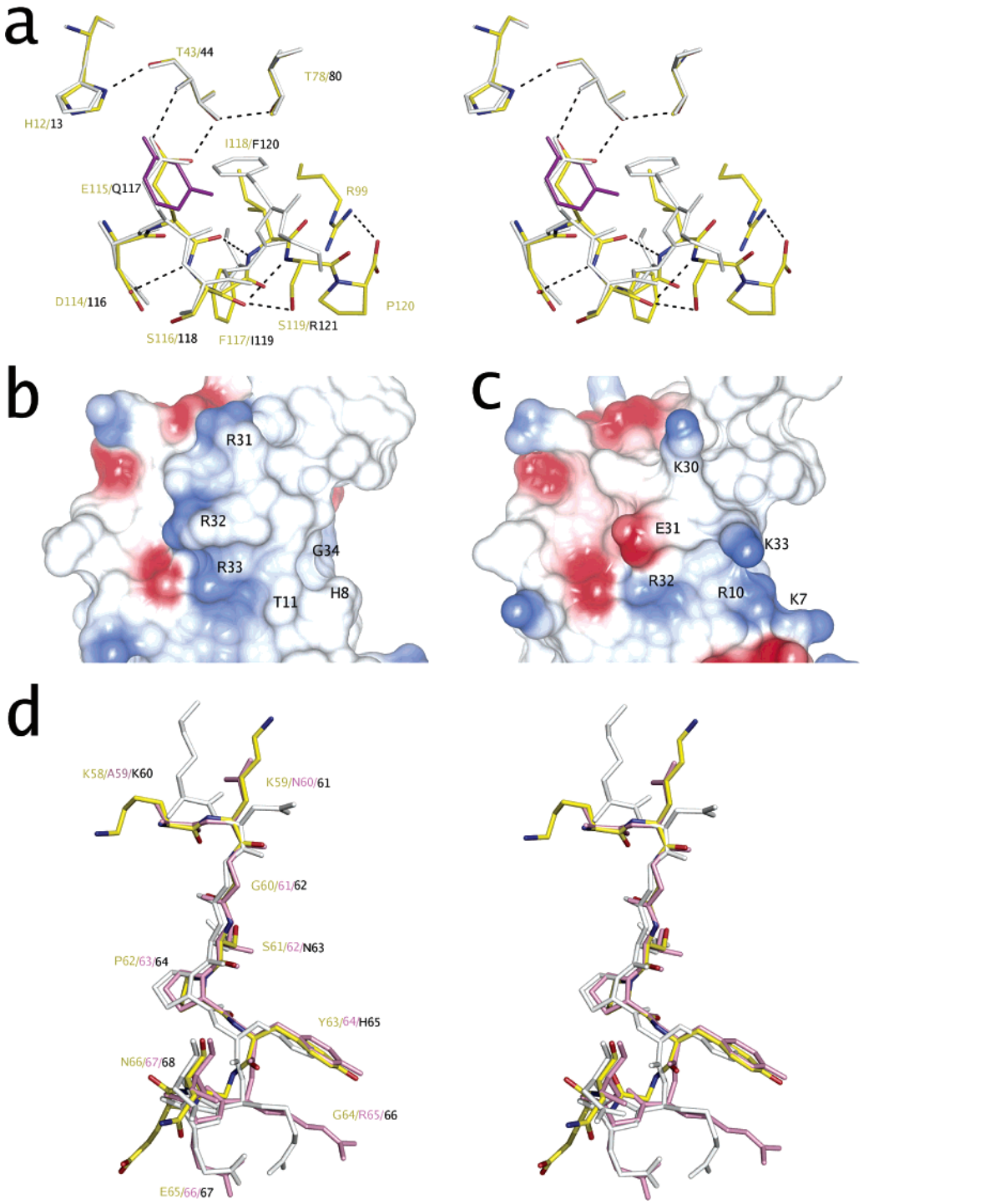

FIGURE 8: Functional regions of mAng-4. (a) Putative B_1 subsite and the obstructive C-terminus. Stereoview in which mAng-4 (carbon, yellow; nitrogen, blue; oxygen, red) is superposed with hAng (pdb entry 1B1I) (*30*) (gray) and a uridine moiety derived from the alignment of mAng-4 with the RNase A−uridine vanadate complex (pdb code 1RUV) (*86*) (purple). The side chain of hAng Arg121 is omitted for clarity. The dashed lines denote potential hydrogen bonds in mAng-4. (b) Nuclear localization sequence and surrounding region of hAng and (c) the corresponding part of mAng-4. Surface representations of electrostatic potential (*68*) in which positively charged, negatively charged, and uncharged atoms are colored blue, red, and white, respectively. (d) Putative cell-binding segment. Stereoview in which mAng-4 (carbon, yellow; nitrogen, blue; oxygen, red) is superposed with hAng (gray) and mAng-1 (pink). In panels (a) and (d), the residue labels for each protein are colored in accordance with the respective carbon atom coloring scheme.

significantly alters the chemical character of the region, and it is unclear why substitutions at these positions are tolerated in mAng-4 but not in hAng.

Mutational Analysis of mAng-4. Several mutants of mAng-4 were prepared with the aim of probing its functional architecture. Their angiogenic and ribonucleolytic activities were assayed and compared with those of the wild-type protein.

H12A- and H112A-mAng-4. In hAng, His13 and His114 comprise two-thirds of the catalytic triad and are integral to the protein's enzymatic and angiogenic activities (*28*). The importance of the two corresponding residues (His12 and

His112) to the function of mAng-4 was tested by mutation to Ala. Either mutation reduced tRNA cleavage activity to the extent that it was undetectable at protein concentrations up to 0.4 μM (Figure 3a), confirming the crucial roles of these two residues in catalysis. This is in accordance with the catalytic inactivity of the equivalent hAng mutants (*28*). Neither H12A- nor H112A-mAng-4 caused a statistically significant change in the proliferation of IGR1 cells (Figure 4c) or in the formation of cellular processes from thoracic aortae (Figure 7a), matching the inactivity of the corresponding hAng mutants on the chicken CAM (*28*). Thus, as with hAng, the ribonucleolytic activity of mAng-4 is required for the elicitation of an angiogenic response.

R32A-mAng-4. In hAng, Arg33 is essential for angiogenesis because of its crucial role in nuclear targeting (*72*). The importance of its counterpart, Arg32, to the function of mAng-4 was evaluated by mutation to Ala. R32A-mAng-4 did not cause a statistically significant change in the proliferation of IGR1 cells (Figure 4c) or in the formation of cellular processes from thoracic aortae (Figure 7a), indicating that this residue is crucial to the angiogenic process. This is consistent with the behavior of the equivalent hAng mutant (R33A), which gives a negative response when assayed on the chicken CAM (*52*). The ribonucleolytic activity of R32A-mAng-4 was indistinguishable from that of wild-type mAng-4 (Figure 3a), indicating that the prepared protein was correctly folded and that this residue does not play a significant role in RNA binding or cleavage. This characteristic differs from that described for R33A-hAng, whose tRNA cleavage activity is 7-fold lower than that of the wild type (*52*). It was previously suggested that the effect of the R33A mutation on the ribonucleolytic activity of hAng could be due to the loss of the hydrogen bonds between the guanidino group of Arg33 and the carbonyl oxygens of Thr11 and Tyr14 located on either side of the catalytic residue His13 (*29*). The crystal structures of mAng-4 and hAng do not provide any clear insight into the differing effects of this mutation on the two proteins. In mAng-4, the guanidino group of Arg32 forms hydrogen bonds with the carbonyl oxygens of Arg10 and Tyr13; the arrangement is identical to that observed for residues Arg33, Thr11, and Tyr14 in hAng. As a consequence of the mutation, some of the space occupied by the arginyl side chain could become available to the side chain of the preceding residue (hAng Arg32 or mAng-4 Glu31, respectively). If so, the greater length of hAng Arg32 would allow a closer approach of this residue to the catalytic site, but a means of interference is not obvious.

K59N-mAng-4. It is possible that differences in the sequence of the cell-binding segment (residues 60−68 of hAng and counterparts) account for some of the differences in the angiogenic potency of various angiogenins. For example, when the sequence of mAng-2 (which is not angiogenic) is compared with those of the hAng, mAng-1, and mAng-3 (which are), Asn → Lys and Glu/Val → Arg replacements are evident at positions 61 and 67, respectively (hAng numbering). Interestingly, mAng-4 possesses the Asn → Lys substitution (at position 59) but not the Glu/Val → Arg change. To determine whether the Asn → Lys replacement has any bearing on the angiogenic potency of mAng-4, we constructed K59N-mAng-4, thereby effecting the reverse substitution.

Surprisingly, K59N-mAng-4 did not stimulate the proliferation of IGR1 cells (Figure 4c) or the formation of cellular processes from thoracic aortae (Figure 7a). The tRNA cleavage activity of K59N-mAng-4 was identical to that of wild-type mAng-4 (Figure 3a), indicating that the prepared protein was correctly folded and that the decrease in angiogenic activity is not attributable to any defect in ribonucleolysis. Thus, from a functional viewpoint, an Asn residue is tolerated poorly at position 59 of the mAng-4 structure, and the contribution of the native Lys residue is positive by comparison.

E115A-mAng-4. Mutational studies on hAng have quantified the contributions of various C-terminal residues to the low ribonucleolytic activity of the protein and to the stability of the B_1 subsite blockage (*76*−*80*). Analysis of the Q117G- and Q117A-hAng mutants has proved to be straightforward: tRNA cleavage activity is increased 30- and 14-fold, respectively, dinucleotide specificity is unchanged, and structural perturbations are localized to the side chain in question (*31*, *78*, *80*). The effect of these mutations on the angiogenic activity of hAng has not been tested. In all murine angiogenins, a Glu residue substitutes at this position (Figure 1a). To determine the functional contribution of this residue (Glu115) in mAng-4, we mutated it to Ala.

The tRNA cleavage activity of E115A-mAng-4 was 15-fold greater than that of wild-type mAng-4 (Figure 3b). This increase closely matches that measured when the corresponding mutation (Q117A) is made to hAng (*80*), suggesting a similar role for this residue in the attenuation of enzymatic activity. Interestingly, E115A-mAng-4 did not stimulate the proliferation of IGR1 cells (Figure 4c) or the formation of cellular processes from thoracic aortae (Figure 7a). Thus, it appears that the angiogenic activity of mAng-4 is dependent on the sufficient suppression of its ribonucleolytic activity.

DISCUSSION

The angiogenin and eosinophil-associated branches of the pancreatic ribonuclease superfamily have expanded remarkably in rodents (*46*). This has raised obvious questions as to whether the biological activities of the various family members are distinct, and whether there are differences in their temporal and spatial regulation. Here, we have demonstrated that mAng-4 is angiogenic, like mAng-1 and mAng-3 (*47*, *48*). Because mAng-4 is expressed primarily in the gut and pancreas (*49*), it may, therefore, play a significant part in the angiogenesis that occurs within these organs. When coupled with its potential role in the intestinal immune system (*37*, *50*), this identifies mAng-4 as an intriguing multi-functional protein.

Our range of assays identified that the stimulatory properties of mAng-4 are dependent on the physiological complexity of the system, as are those of hAng and mAng-1. In a simple proliferation assay employing sparse cultures of BCE or MEF cells, the angiogenins were inactive (Figure 4a and b). This matches the behavior of bovine aortic endothelial (BAE) cells after exposure to hAng or bovine Ang (bAng) (*81*) but not that of endothelial cells from bovine brain capillaries or the human umbilical vein, both of which proliferate significantly in response to hAng after starving of serum and bFGF (*81*−*83*). This confirms that the

proliferative response of cultured cells to angiogenins is highly cell type specific. When the two non-transformed cell lines were replaced with IGR1 human melanoma cells, the angiogenins induced a proliferative response (Figure 4c). Differences in the responsiveness of different cell lines may be due to differing expressions of Ang receptors on the cell surface and/or differing requirements for other angiogenic or growth factors that can act in concert with Ang.

hAng stimulates the proteolytic activities of bovine endothelial cells associated with cell invasion and promotes their invasiveness (*19*). Furthermore, bovine Ang (bAng) stimulates the migration of BAE cells in culture (*20*). However, in our migration assay involving cultured BCE or MEF cells, angiogenins were inactive (Figure 5). This may be due to the same cell type differences that govern the proliferative response.

In the bead-based and thoracic aorta assays, GFR Matrigel served as a model of the extracellular matrix (ECM). Matrigel is extracted from Engelbreth−Holm−Swarm mouse sarcoma cells and contains a range of ECM proteins, including laminin, collagen IV, heparin sulfate proteoglycans, and entactin. It is a more complete model of the ECM than single-component gels, such as fibrinogen or collagen, and, therefore, more closely mimics the environment *in vivo*. Angiogenins did not induce the sprouting of cellular processes from BCE cells grown on Cytodex 3 beads (Figure 6), which may indicate a requirement for pre-existing vasculature or simply for endothelial cells of a specific origin. In support of the latter, bAng has been shown to induce tubular morphogenesis of BAE cells embedded in collagen gel (*20*). Angiogenins did, however, induce sprouting from sections of thoracic aorta (Figure 7). Although in widespread use for the assay of angiogenic and anti-angiogenic compounds (*84*), this is the first time that the thoracic aorta system has been used for angiogenins. It offers several major advantages over the other angiogenesis assay systems that have been used for angiogenins, that is, the chicken CAM, rabbit cornea, and rabbit knee meniscus. Of these systems, only the CAM assay has been used routinely because the cornea assay is generally discredited in the field, and the knee meniscus assay is so cumbersome and expensive that it cannot be routinely applied. Compared to the CAM assay, the thoracic aorta assay is more technically straightforward and more quantitative. It also offers an advantage in that it uses a mammalian system, the importance of which has come to light over the past few years as work on the chicken genome has failed to reveal a clear orthologue of human/murine Ang, potentially undermining the relevance of results obtained with the CAM assay. In view of these advantages, the thoracic aorta assay should prove to be invaluable for studies on human as well as murine angiogenins.

As might be expected from sequence homology alone, the crystal structure of mAng-4 is extremely similar to that of mAng-1 and hAng. Importantly, the structure permits the interpretation of most of our site-directed mutagenesis data with some confidence. First, the identity and positioning of residues that are likely to participate in RNA binding and cleavage are well conserved. Hence, it can be safely assumed that the angiogenic inactivity of the H12A and H112A mutants is an indication of the dependence of the angiogenic activity of mAng-4 on the exertion of its ribonucleolytic activity, as has been demonstrated for hAng (*28*). Second, although the NLS is present in modified form, Arg32 is maintained in the same position as the major nuclear translocation determinant of hAng, Arg33. The activity of the R32A mutant indicates that this residue is also essential to the angiogenic process, most likely participating in nuclear translocation. Third, the putative B_1 subsite is blocked by Glu115, the counterpart of Q117 in hAng. The E115A mutation increases ribonucleolytic activity but abolishes angiogenic activity, effectively decoupling the two. Given that a similar modification of hAng (Q117G) brings about a highly localized reduction in blockage (*31*) and that the mutation site is distant from any region implicated in cell binding or nuclear translocation, the angiogenic inactivity of this mutant can be directly attributed to its increased ribonucleolytic activity. This is the second time that such an effect has been observed, the previous instance involving another enzymatically superactive hAng mutant, ARH-II (*85*). Because it is possible that the ribonucleolytic activity of Ang is employed for the processing of pre-rRNA into ribosomes (*24*), nonspecific degradation of this or some other RNA substrate may underlie the reduced biological activity of ARH-II (*33*) and E117A-mAng-4.

The dramatic effect of the K59N mutation on angiogenic activity confirms that angiogenins are highly sensitive to modification in this putative cell-binding region. However, given that the mutation simply changes this residue to the one found in the sequences of hAng and mAng-1, the abolition of angiogenic activity is most unexpected. It is possible that there is a general requirement for more than one basic residue in the cell-binding segment, which is not fulfilled after the mutation (Figure 8d). Alternatively, an Asn residue introduced at this position in mAng-4 may interact strongly with a neighboring residue and be unavailable for intermolecular contact. Determination of the X-ray crystal structure of K59N-mAng-4 will be necessary to resolve this issue.

ACKNOWLEDGMENT

We thank the staff at the Synchrotron Radiation Source, Daresbury (U.K.), Nethaji Thiyagarajan and Shalini Iyer, for their help with X-ray data collection. We thank Michelle Hares for help in the production of murine Ang proteins during the early part of this work.

REFERENCES

1. Strydom, D. J., Fett, J. W., Lobb, R. R., Alderman, E. M., Bethune, J. L., Riordan, J. F., and Vallee, B. L. (1985) Amino acid sequence of human tumor derived angiogenin, *Biochemistry 24*, 5486−5494.
2. Beintema, J. J., Breukelman, H. J., Carsana, A., and Furia, A. (1997) Evolution of Vertebrate Ribonucleases: Ribonuclease A Superfamily, in *Ribonucleases: Structures and Functions* (D'Alessio, G., and Riordan, J. F., Eds.), pp 245−269, Academic Press, New York.
3. Adams, S. A., and Subramanian, V. (1999) The angiogenins: an emerging family of ribonuclease related proteins with diverse cellular functions, *Angiogenesis 3*, 189−199.
4. Fett, J. W., Strydom, D. J., Lobb, R. R., Alderman, E. M., Bethune, J. L., Riordan, J. F., and Vallee, B. L. (1985) Isolation and characterization of angiogenin, an angiogenic protein from human carcinoma cells, *Biochemistry 24*, 5480−5486.
5. King, T. V., and Vallee, B. L. (1991) Neovascularisation of the meniscus with angiogenin. An experimental study in rabbits, *J. Bone Jt Surg., Br. Vol. 73*, 587−590.
6. Shapiro, R., Strydom, D. J., Olson, K. A., and Vallee, B. L. (1987) Isolation of angiogenin from normal human plasma, *Biochemistry 26*, 5141−5146.

7. Maes, P., Damart, D., Rommens, C., Montreuil, J., Spik, G., and Tartar, A. (1988) The complete amino acid sequence of bovine milk angiogenin, *FEBS Lett. 241*, 41−45.
8. Moenner, M., Gusse, M., Hatzi, E., and Badet, J. (1994) The widespread expression of angiogenin in different human cells suggests a biological function not only related to angiogenesis, *Eur. J. Biochem. 226*, 483−490.
9. Rajashekhar, G., Loganath, A., Roy, A. C., and Wong, Y. C. (2002) Expression and localization of angiogenin in placenta: enhanced levels at term over first trimester villi, *Mol. Reprod. Dev. 62*, 159−166.
10. Pavlov, N., Hatzi, E., Bassaglia, Y., Frendo, J. L., Brion, D. E., and Badet, J. (2003) Angiogenin distribution in human term placenta, and expression by cultured trophoblastic cells, *Angiogenesis 6*, 317−330.
11. Olson, K. A., French, T. C., Vallee, B. L., and Fett, J. W. (1994) A monoclonal antibody to human angiogenin suppresses tumor growth in athymic mice, *Cancer Res. 54*, 4576−4579.
12. Olson, K. A., Fett, J. W., French, T. C., Key, M. E., and Vallee, B. L. (1995) Angiogenin antagonists prevent tumor growth *in vivo*, *Proc. Natl. Acad. Sci. U.S.A. 92*, 442−446.
13. Olson, K. A., Byers, H. R., Key, M. E., and Fett, J. W. (2001) Prevention of human prostate tumor metastasis in athymic mice by antisense targeting of human angiogenin, *Clin. Cancer Res. 7*, *3598*−3605.
14. Olson, K. A., Byers, H. R., Key, M. E., and Fett, J. W. (2002) Inhibition of prostate carcinoma establishment and metastatic growth in mice by an antiangiogenin monoclonal antibody, *Int. J. Cancer 98*, 923−929.
15. Kao, R. Y., Jenkins, J. L., Olson, K. A., Key, M. E., Fett, J. W., and Shapiro, R. (2002) A small-molecule inhibitor of the ribonucleolytic activity of human angiogenin that possesses antitumor activity, *Proc. Natl. Acad. Sci. U.S.A. 99*, 10066−10071.
16. Bicknell, R., and Vallee, B. L. (1988) Angiogenin activates endothelial cell phospholipase C, *Proc. Natl. Acad. Sci. U.S.A. 85*, 5961−5965.
17. Bicknell, R., and Vallee, B. L. (1989) Angiogenin stimulates endothelial cell prostacyclin secretion by activation of phospholipase A2, *Proc. Natl. Acad. Sci. U.S.A. 86*, 1573−1577.
18. Soncin, F. (1992) Angiogenin supports endothelial and fibroblast cell adhesion, *Proc. Natl. Acad. Sci. U.S.A. 89*, 2232−2236.
19. Hu, G., Riordan, J. F., and Vallee, B. L. (1994) Angiogenin promotes invasiveness of cultured endothelial cells by stimulation of cell-associated proteolytic activities, *Proc. Natl. Acad. Sci. U.S.A. 91*, 12096−12100.
20. Jimi, S., Ito, K., Kohno, K., Kuwano, M., Itagaki, Y., and Ishikawa, H. (1995) Modulation by bovine angiogenin of tubular morphogenesis and expression of plasminogen activator in bovine endothelial cells, *Biochem. Biophys. Res. Commun. 211*, 476−483.
21. Hu, G. F., Riordan, J. F., and Vallee, B. L. (1997) A putative angiogenin receptor in angiogenin-responsive human endothelial cells, *Proc. Natl. Acad. Sci. U.S.A. 94*, 2204−2209.
22. Moroianu, J., and Riordan, J. F. (1994) Nuclear translocation of angiogenin in proliferating endothelial cells is essential to its angiogenic activity, *Proc. Natl. Acad. Sci. U.S.A. 91*, 1677−1681.
23. Hu, G., Xu, C., and Riordan, J. F. (2000) Human angiogenin is rapidly translocated to the nucleus of human umbilical vein endothelial cells and binds to DNA, *J. Cell. Biochem. 76*, 452−462.
24. Xu, Z. P., Tsuji, T., Riordan, J. F., and Hu, G. F. (2002) The nuclear function of angiogenin in endothelial cells is related to rRNA production, *Biochem. Biophys. Res. Commun. 294*, 287−292.
25. Kishimoto, K., Liu, S., Tsuji, T., Olson, K. A., and Hu, G. F. (2005) Endogenous angiogenin in endothelial cells is a general requirement for cell proliferation and angiogenesis, *Oncogene 24*, 445−456.
26. Shapiro, R., Riordan, J. F., and Vallee, B. L. (1986) Characteristic ribonucleolytic activity of human angiogenin, *Biochemistry 25*, 3527−3532.
27. Harper, J. W., and Vallee, B. L. (1989) A covalent angiogenin/ribonuclease hybrid with a fourth disulfide bond generated by regional mutagenesis, *Biochemistry 28*, 1875−1884.
28. Shapiro, R., and Vallee, B. L. (1989) Site-directed mutagenesis of histidine-13 and histidine-114 of human angiogenin. Alanine derivatives inhibit angiogenin-induced angiogenesis, *Biochemistry 28*, 7401−7408.
29. Acharya, K. R., Shapiro, R., Allen, S. C., Riordan, J. F., and Vallee, B. L. (1994) Crystal structure of human angiogenin reveals the structural basis for its functional divergence from ribonuclease, *Proc. Natl. Acad. Sci. U.S.A. 91*, 2915−2919.
30. Leonidas, D. D., Shapiro, R., Allen, S. C., Subbarao, G. V., Veluraja, K., and Acharya, K. R. (1999) Refined crystal structures of native human angiogenin and two active site variants: implications for the unique functional properties of an enzyme involved in neovascularisation during tumour growth, *J. Mol. Biol. 285*, 1209−1233.
31. Leonidas, D. D., Shapiro, R., Subbarao, G. V., Russo, A., and Acharya, K. R. (2002) Crystallographic studies on the role of the C-terminal segment of human angiogenin in defining enzymatic potency, *Biochemistry 41*, 2552−2562.
32. Holloway, D. E., Shapiro, R., Hares, M. C., Leonidas, D. D., and Acharya, K. R. (2002) Guest−host crosstalk in an angiogenin−RNase A chimeric protein, *Biochemistry 41*, 10482−10489.
33. Holloway, D. E., Chavali, G. B., Hares, M. C., Baker, M. D., Subbarao, G. V., Shapiro, R., and Acharya, K. R. (2004) Crystallographic studies on structural features that determine the enzymatic specificity and potency of human angiogenin: Thr44, Thr80, and residues 38−41, *Biochemistry 43*, 1230−1241.
34. Greenway, M. J., Alexander, M. D., Ennis, S., Traynor, B. J., Corr, B., Frost, E., Green, A., and Hardiman, O. (2004) A novel candidate region for ALS on chromosome 14q11.2, *Neurology 63*, 1936−1938.
35. Greenway, M. J., Andersen, P. M., Russ, C., Ennis, S., Cashman, S., Donaghy, C., Patterson, V., Swingler, R., Kieran, D., Prehn, J., Morrison, K. E., Green, A., Acharya, K. R., Brown, R. H., Jr, and Hardiman, O. (2006) ANG mutations segregate with familial and 'sporadic' amyotrophic lateral sclerosis, *Nat. Genet. 38*, 411−413.
36. Olson, K. A., Verselis, S. J., and Fett, J. W. (1998) Angiogenin is regulated *in vivo* as an acute phase protein, *Biochem. Biophys. Res. Commun. 242*, 480−483.
37. Hooper, L. V., Stappenbeck, T. S., Hong, C. V., and Gordon, J. I. (2003) Angiogenins: a new class of microbicidal proteins involved in innate immunity, *Nat. Immunol. 4*, 269−273.
38. Matoušek, J., Souček, J., Říha, J., Zankel, T. R., and Benner, S. A. (1995) Immunosuppresive activity of angiogenin in comparison with bovine seminal ribonuclease and pancreatic ribonuclease, *Comp. Biochem. Physiol., B 112*, 235−241.
39. Tschesche, H., Kopp, C., Horl, W. H., and Hempelmann, U. (1994) Inhibition of degranulation of polymorphonuclear leukocytes by angiogenin and its tryptic fragment, *J. Biol. Chem. 269*, 30274−30280.
40. Schmaldienst, S., Oberpichler, A., Tschesche, H., and Horl, W. H. (2003) Angiogenin: a novel inhibitor of neutrophil lactoferrin release during extracorporeal circulation, *Kidney Blood Pressure Res. 26*, 107−112.
41. Bond, M. D., and Vallee, B. L. (1990) Isolation and sequencing of mouse angiogenin DNA, *Biochem. Biophys. Res. Commun. 171*, 988−995.
42. Holloway, D. E., Chavali, G. B., Hares, M. C., Subramanian, V., and Acharya, K. R. (2005) Structure of murine angiogenin: features of the substrate- and cell-binding regions and prospects for inhibitor-binding studies, *Acta. Crystallogr., Sect. D 61*, 1568−1578.
43. Brown, W. E., Nobile, V., Subramanian, V., and Shapiro, R. (1995) The mouse angiogenin gene family: structures of an angiogenin-related protein gene and two pseudogenes, *Genomics 29*, 200−206.
44. Fu, X., and Kamps, M. P. (1997) E2a-Pbx1 induces aberrant expression of tissue-specific and developmentally regulated genes when expressed in NIH 3T3 fibroblasts, *Mol. Cell. Biol. 17*, 1503−1512.
45. Strydom, D. J. (1998) The angiogenins, *Cell Mol. Life Sci. 54*, 811−824.
46. Cho, S., Beintema, J. J., and Zhang, J. (2005) The ribonuclease A superfamily of mammals and birds: identifying new members and tracing evolutionary histories, *Genomics 85*, 208−220.
47. Nobile, V., Vallee, B. L., and Shapiro, R. (1996) Characterization of mouse angiogenin-related protein: implications for functional studies on angiogenin, *Proc. Natl. Acad. Sci. U.S.A. 93*, 4331−4335.
48. Fu, X., Roberts, W. G., Nobile, V., Shapiro, R., and Kamps, M. P. (1999) mAngiogenin-3, a target gene of oncoprotein E2a-Pbx1, encodes a new angiogenic member of the angiogenin family, *Growth Factors 17*, 125−137.

49. Birney, E., Andrews, D., Caccamo, M., Chen, Y., Clarke, L., Coates, G., Cox, T., Cunningham, F., Curwen, V., Cutts, T., Down, T., Durbin, R., Fernandez-Suarez, X. M., Flicek, P., Graf, S., Hammond, M., Herrero, J., Howe, K., Iyer, V., Jekosch, K., and Kahari, A., et al. (2006) Ensembl 2006, *Nucleic Acids Res. 34*, D556−D561.
50. Stappenbeck, T. S., Hooper, L. V., and Gordon, J. I. (2002) Developmental regulation of intestinal angiogenesis by indigenous microbes via Paneth cells, *Proc. Natl. Acad. Sci. U.S.A. 99*, 15451−15455.
51. Rawls, J. F., Samuel, B. S., and Gordon, J. I. (2004) Gnotobiotic zebrafish reveal evolutionarily conserved responses to the gut microbiota, *Proc. Natl. Acad. Sci. U.S.A. 101*, 4596−4601.
52. Shapiro, R., and Vallee, B. L. (1992) Identification of functional arginines in human angiogenin by site-directed mutagenesis, *Biochemistry 31*, 12477−12485.
53. Holloway, D. E., Hares, M. C., Shapiro, R., Subramanian, V., and Acharya, K. R. (2001) High-level expression of three members of the murine angiogenin family in *Escherichia coli* and purification of the recombinant proteins, *Protein Expression Purif. 22*, 307−317.
54. Shapiro, R., Harper, J. W., Fox, E. A., Jansen, H. W., Hein, F., and Uhlmann, E. (1988) Expression of Met-(−1) angiogenin in *Escherichia coli*: conversion to the authentic <Glu-1 protein, *Anal. Biochem. 175*, 450−461.
55. Hogan, B., Beddington, R., Constantini., F., and Lacy, E. (1994) *Manipulating the Mouse Embryo: A Laboratory Manual*, 2nd ed., Cold Spring Harbor Press, Cold Spring Harbor, NY.
56. Nehls, V., and Drenckhahn, D. (1995) A microcarrier-based cocultivation system for the investigation of factors and cells involved in angiogenesis in three-dimensional fibrin matrices *in vitro*, *Histochem. Cell Biol. 104*, 459−466.
57. Masson, V., Devy, L., Grignet-Debrus, C., Bernt, S., Bajou, K., Blacher, S., Roland, G., Chang, Y., Fong, T., Carmeliet, P., Foidart, J.-M., and Noël, A. (2002) Mouse aortic ring assay: a new approach of the molecular genetics of angiogenesis, *Biol. Proced. Online 4*, 24−31.
58. Shapiro, R., Weremowicz, S., Riordan, J. F., and Vallee, B. L. (1987) Ribonucleolytic activity of angiogenin: essential histidine, lysine, and arginine residues, *Proc. Natl. Acad. Sci. U.S.A. 84*, 8783−8787.
59. Otwinowski, Z., and Minor, W. (1997) Processing of X-ray diffraction data collected in oscillation mode, *Methods Enzymol. 276*, 307−326.
60. Navaza, J. (1994) AMoRe: an automated package for molecular replacement, *Acta Crystallogr., Sect. D 50*, 157−163.
61. Brünger, A. T., Adams, P. D., Clore, G. M., DeLano, W. L., Gros, P., GrosseKunstleve, R. W., Jiang, J. S., Kuszewski, J., Nilges, M., Pannu, N. S., Read, R. J., Rice, L. M., Simonson, T., and Warren, G. L. (1998) Crystallography & NMR System: a new software suite for macromolecular structure determination, *Acta Crystallogr., Sect. D 54*, 905−921.
62. Brünger, A. T. (1992) Free *R* value: a novel statistical quantity for assessing the accuracy of crystal structures, *Nature 355*, 472−475.
63. Jones, T. A., Zou, J.-Y., Cowan, S. W., and Kjeldgaard, M. (1991) Improved methods for binding protein models in electron density maps and the location of errors in these models, *Acta Crystallogr., Sect. A 47*, 110−119.
64. Hooft, R. W., Vriend, G., Sander, C., and Abola, E. E. (1996) Errors in protein structures, *Nature 381*, 272.
65. Laskowski, R. A., MacArthur, M. W., Moss, D. S., and Thornton, J. M. (1993) PROCHECK: a program to check the stereochemical quality of protein structures, *J. Appl. Crystallogr. 26*, 283−291.
66. Bailey, S. (1994) The CCP4 suite: programs for protein crystallography, *Acta Crystallogr., Sect. D 50*, 760−763.
67. Davis, I. W., Murray, L. W., Richardson, J. S., and Richardson, D. C. (2004) MOLPROBITY: structure validation and all-atom contact analysis for nucleic acids and their complexes, *Nucleic Acids Res. 32*, W615−W619.
68. Potterton, L., McNicholas, S., Krissinel, E., Gruber, J., Cowtan, K., Emsley, P., Murshudov, G. N., Cohen, S., Perrakis, A., and Noble, M. (2004) Developments in the *CCP*4 molecular-graphics project, *Acta Crystallogr., Sect. D 60*, 2288−2294.
69. Raines, R. T. (1998) Ribonuclease A, *Chem. Rev. 98*, 1045−1065.
70. Parés, X., Nogués, M. V., de Llorens, R., and Cuchillo, C. M. (1991) Structure and function of ribonuclease A binding subsites, *Essays Biochem. 26*, 89−103.
71. Acharya, K. R., Shapiro, R., Riordan, J. F., and Vallee, B. L. (1995) Crystal structure of bovine angiogenin at 1.5-Å resolution, *Proc. Natl. Acad. Sci. U.S.A. 92*, 2949−2953.
72. Moroianu, J., and Riordan, J. F. (1994) Identification of the nucleolar targeting signal of human angiogenin, *Biochem. Biophys. Res. Commun. 203*, 1765−1772.
73. Jans, D. A., Xiao, C. Y., and Lam, M. H. (2000) Nuclear targeting signal recognition: a key control point in nuclear transport? *BioEssays 22*, 532−544.
74. Hallahan, T. W., Shapiro, R., and Vallee, B. L. (1991) Dual site model for the organogenic activity of angiogenin, *Proc. Natl. Acad. Sci. U.S.A. 88*, 2222−2226.
75. Hallahan, T. W., Shapiro, R., Strydom, D. J., and Vallee, B. L. (1992) Importance of asparagine-61 and asparagine-109 to the angiogenic activity of human angiogenin, *Biochemistry 31*, 8022−8029.
76. Harper, J. W., and Vallee, B. L. (1988) Mutagenesis of aspartic acid-116 enhances the ribonucleolytic activity and angiogenic potency of angiogenin, *Proc. Natl. Acad. Sci. U.S.A. 85*, 7139−7143.
77. Curran, T. P., Shapiro, R., and Riordan, J. F. (1993) Alteration of the enzymatic specificity of human angiogenin by site-directed mutagenesis, *Biochemistry 32*, 2307−2313.
78. Russo, N., Shapiro, R., Acharya, K. R., Riordan, J. F., and Vallee, B. L. (1994) Role of glutamine-117 in the ribonucleolytic activity of human angiogenin, *Proc. Natl. Acad. Sci. U.S.A. 91*, 2920−2924.
79. Russo, N., Nobile, V., Di, Donato, A., Riordan, J. F., and Vallee, B. L. (1996) The C-terminal region of human angiogenin has a dual role in enzymatic activity, *Proc. Natl. Acad. Sci. U.S.A. 93*, 3243−3247.
80. Shapiro, R. (1998) Structural features that determine the enzymatic potency and specificity of human angiogenin: threonine-80 and residues 58−70 and 116−123, *Biochemistry 37*, 6847−6856.
81. Chamoux, M., Dehouck, M. P., Fruchart, J. C., Spik, G., Montreuil, J., and Cecchelli, R. (1991) Characterization of angiogenin receptors on bovine brain capillary endothelial cells, *Biochem. Biophys. Res. Commun. 176*, 833−839.
82. Hu, G. F. (1998) Neomycin inhibits angiogenin-induced angiogenesis, *Proc. Natl. Acad. Sci. U.S.A. 95*, 9791−9795.
83. Liu, S., Yu, D., Xu, Z. P., Riordan, J. F., and Hu, G. F. (2001) Angiogenin activates Erk1/2 in human umbilical vein endothelial cells, *Biochem. Biophys. Res. Commun. 287*, 305−310.
84. Go, R. S., and Owen, W. C. (2003) The rat aortic ring assay for *in vitro* study of angiogenesis, *Methods Mol. Med. 85*, 59−64.
85. Harper, J. W., Fox, E. A., Shapiro, R., and Vallee, B. L. (1990) Mutagenesis of residues flanking Lys-40 enhances the enzymatic activity and reduces the angiogenic potency of angiogenin, *Biochemistry 29*, 7297−7302.
86. Ladner, J. E., Wladkowski, B. D., Svensson, L. A., Sjölin, L., and Gilliland, G. L. (1997) X-ray structure of a ribonuclease A−uridine vanadate complex at 1.3 Å resolution, *Acta Crystallogr., Sect. D 53*, 290−301.

BI062158N